**Applied
Magnetic Resonance**

CrossMark

ORIGINAL PAPER

EPR Uniform Field Signal Enhancement by Dielectric Tubes in Cavities

James S. Hyde[1] · **Richard R. Mett[1,2]**

Abstract The dielectric tube resonator (DTR) for electron paramagnetic resonance spectroscopy is introduced. It is defined as a metallic cylindrical TE_{011} microwave cavity that contains a dielectric tube centered on the axis of the cylinder. Contour plots of dimensions of the metallic cylinder to achieve resonance at 9.5 GHz are shown for quartz, sapphire, and rutile tubes as a function of wall thickness and average radius. These contour plots were developed using analytical equations and confirmed by finite-element modeling. They can be used in two ways: design of the metallic cylinder for use at 9.5 GHz that incorporates a readily available tube such as a sapphire tube intended for NMR and design of a custom procured tube for optimized performance for specific sample-size constraints. The charts extend to the limiting condition where the dielectric fills the tube. However, the structure at this limit is not a dielectric resonator due to the metal wall and does not radiate. In addition, the uniform field (UF) DTR is introduced. Development of the UF resonator starting with a DTR is shown. The diameter of the tube remains constant along the cavity axis, and the diameter of the cylindrical metallic enclosure increases at the ends of the cavity to satisfy the uniform field condition. This structure has advantages over the previously developed UF TE_{011} resonators: higher resonator efficiency parameter Λ, convenient overall size when using sapphire tubes, and higher quality data for small samples. The DTR and UF DTR structures fill the gap between free space and dielectric resonator limits in a continuous manner.

✉ James S. Hyde
  jshyde@mcw.edu

[1] Department of Biophysics, Medical College of Wisconsin, 8701 Watertown Plank Road, Milwaukee, WI 53226, USA

[2] Department of Physics and Chemistry, Milwaukee School of Engineering, 1025 North Broadway, Milwaukee, WI 53202, USA

1 Introduction

The Varian "Multi-purpose" X-band microwave cavity for use in electron paramagnetic resonance (EPR) was introduced by Rempel et al. [1] in a US patent application filed on December 21, 1959, and issued on February 25, 1964. This structure oscillated in the rectangular TE_{102} mode, where the indices correspond to x, y, and z in rectangular coordinates. In normal usage, the z-axis (index 2) was horizontal and perpendicular to the applied magnetic field H_0, which was along the y-axis (index 0). So-called "stacks," which were cylindrical metallic tubes of 11 mm inner diameter, were centered in the y–z planes on the top and bottom surfaces. The patent application remarks that these stacks were beyond cutoff, and microwave energy did not leak out. The cavity Q value remained high, and the stacks provided convenient access to the interior of the cavity. A feature of this cavity was that a double-walled Dewar made from concentric, thin-walled quartz tubes could be inserted through these stacks. The sample was placed in the Dewar and temperature control of the sample was achieved by regulated gas flowing over the sample. Temperature control of the sample while the microwave structure remained at room temperature was a central claim of the patent.

It was soon discovered that the presence of the quartz Dewar insert resulted in an increase in EPR signal intensity even though the Dewar and sample remained at room temperature. Insertion of the Dewar resulted in a decrease in the microwave frequency from 9.5 to 8.8 GHz, which one might have thought would lead to a decrease in signal because of reduced Zeeman splitting. Apparently, the interaction of the quartz, which has a dielectric constant of 3.8, with the microwave electric field led to a change in the distribution of the microwave magnetic field, as might be expected from the coupling of H and E through Maxwell's equations. Hyde reports enhancement through Dewar insertion of a factor of 2 for samples that do not exhibit microwave power saturation and a factor of $2^{1/2}$ for samples that do (see Table 4 in Ref. [2]). (In the latter case, it is assumed that the incident microwave power in the presence of the Dewar was readjusted to the level that was incident on the sample in the absence of the Dewar).

In a separate application of the multi-purpose cavity, the presence of the stacks centered in the y–z plane led to the development of the so-called "flat cell," usually made from quartz, which constrained an aqueous EPR sample to the nodal x–y plane, where the radiofrequency (rf) electric field passes through zero intensity. Stoodley studied this geometry and observed that the presence of the aqueous flat cell increased the intensity of the rf magnetic field [3]. He called it the "sucking-in" effect.

There are two very widely used resonant cavity modes for EPR, the rectangular TE_{102} and the cylindrical TE_{011}. The Varian version of the cylindrical resonator is described in more detail in Refs. [4, 5]. It also employed "stacks" centered on the end surfaces. They were configured to use the same Dewar accessories that were developed for the multi-purpose rectangular cavity. Again, enhancement of the EPR signal intensity was observed. The motivation of this paper is to understand and optimize the signal enhancement. We restrict our attention to the cylindrical

geometry. Thus, we are concerned with cylindrical sample tubes placed in cylindrical dielectric tubes of various diameters and dielectric constants that are centered in the cylindrical TE_{011} cavity resonator. In the analytical approach, the diameter-to-length ratio (D/L) of the overall resonator is held to unity, and D and L are reset to maintain resonance at 9.5 GHz.

In the limit that the resonator is filled with dielectric, we would appear to reach the dielectric resonator (DR) limit. However, additional losses from currents induced in the metallic boundary lower the Q value because evanescent fields of the DR cannot penetrate the metallic surrounding. These losses gradually decrease as the dielectric tube diameter decreases and the fields at the surface of the surrounding metallic wall diminish.

The present work can be distinguished from the extensive body of work on DRs [6–24] by the tube extending axially from cavity wall to cavity wall. This makes the calculation expressible analytically in closed form, unlike the DR, which is surrounded by evanescent fields [25–27]. In addition, there is no mode splitting [18, 19, 21]. The calculation is exact for any aspect ratio of the tube or cavity. The theory of the dielectric cavity resonator of Rosenbaum [28] is extended to include a conducting wall enclosing the tube.

The principle behind the design of "stacks" for Dewar and sample insertion is to recognize that the stacks can be considered as waveguides, usually cylindrical, but possibly rectangular. Propagation of microwave power in the stacks occurs in modes, each described by an index pair, with each mode characterized by a cut-off frequency. In addition, the symmetry of the microwave fields in the resonator must be such that a given mode is excited for undesirable leakage to occur. A US patent covering these issues, now long expired, supplements the original patent of Rempel et al. [1, 29]. For the cylindrical TE_{011} mode at X-band, a stack diameter of 25 mm was successful in a commercial Varian design. (See Ref. [30] for an exploded view of the actual "large sample access" configuration).

In the present paper, we wished to separate the design aspects of the effect of dielectric tubes on the fields within the resonator from the effect on possible fields in the stacks. Therefore, in the simulations considered here, the metallic boundaries in the x–y planes were continuous, with no stacks and no provision for Dewar insertion or sample entry. The figure of merit used here for resonator comparison was the resonator efficiency parameter, Λ, which was introduced by Hyde [31], where $\Lambda = H_1/(P_0)^{1/2}$, to overcome problems in the standard approach of Feher to analyze spectrometer sensitivity [32].

Feher showed that the EPR continuous wave signal, S, when employing linear detection of the microwave carrier, can be written as

$$S = S_0 Q \eta \chi P_0^{1/2}, \tag{1}$$

where S_0 characterizes the instrument, Q is a measure of the stored energy in the resonator at match, divided by the energy lost per cycle, P_0 is the incident microwave power, and χ is the rf susceptibility as described by the stationary solution to the Bloch equations. The term η is called the filling factor. It is given by the energy stored in the magnetic field integrated over the sample volume divided

by the energy stored in the cavity. There are two problems with this formulation: the filling factor is an integral that is not directly measurable, and the formulation fails as P_0 increases because χ becomes increasingly nonlinear as microwave power saturation occurs.

Hyde rewrote the formulation as

$$S_1/S_2 = \Lambda_1^2/\Lambda_2^2, \tag{2}$$

for comparison of signal heights in different resonators under the assumption that signals do not saturate at the maximum available microwave power, and

$$S_1/S_2 = \Lambda_1/\Lambda_2, \tag{3}$$

for samples that do exhibit partial saturation. In this case, the incident power is assumed to be readjusted to maintain H_1 at the sample constant. The value of H_1 is assumed to be uniform over the sample volume V, which is assumed to be the same in the two resonators being compared. This formulation provides relative sensitivities at a small but finite point. It is rigorous if the field is uniform over the sample. Equations (2) and (3) are readily scaled by the ratio V_1/V_2 if samples of different volume are under comparison and fields are uniform over the sample in both cases.

Thus, in the simulations performed in the present work for the cylindrical TE_{011} mode resonator, the logic progression was as follows:

- Assume a dielectric tube of average diameter d and wall thickness t.
- Let the dielectric constant ε be 4, 10, or 100 (nominal values for quartz, sapphire, and rutile [titanium dioxide, TiO_2], respectively).
- Assume a cavity-diameter-to-length ratio of value 1.
- Find a resonator diameter such that the resonance frequency is 9.5 GHz with the dielectric tube abutting the two inner x–y planes.
- Calculate the resonator efficiency parameter Λ for each assumed value of the dielectric constant at the geometric center of the structure in a three-dimensional display of Λ vs t and d.

The overriding rationale for development of the loop-gap resonator (LGR) [33] was to make the capacitance of the gap as large as possible, forcing the inductance to be small within the general lumped circuit resonance condition $\omega^2 LC = 1$, and to satisfy this condition at microwave frequencies by making the structure quite small. This development led to optimization of EPR performance for small samples. The rationale for the development presented here is similar but is carried out in the vocabulary of distributed circuits. A dielectric tube is placed in the region of the electric field standing wave in a resonant cavity oscillating in the cylindrical TE_{011} mode, which forces the overall dimensions of the cavity to become small if the resonant frequency is to remain unchanged. It is a new perspective, and the overall benefits of such an approach are uncertain.

Figure 1 is brought forward from Sect. 3 for increased clarity of the structure of this paper. It shows simulations of electric and magnetic rf fields at X-band (9.5 GHz) in a cylindrical TE_{011} cavity that contains along the axis a rutile tube. The tube was 3.5 mm outer diameter and 1.5 mm inner diameter. Resonance was achieved at 9.5 GHz when both diameter and length of the cavity, and also the
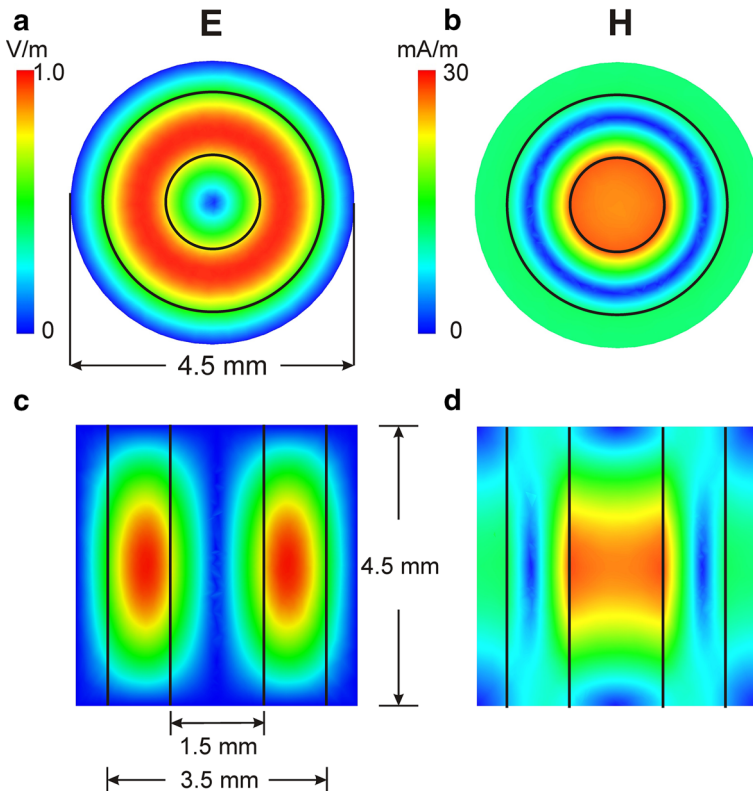
Fig. 1 Cross-sectional views of the magnitude of **a**, **c** electric field and **b**, **d** magnetic field inside a metallic cavity partly filled with a polycrystalline rutile dielectric tube. The electric field is primarily in the dielectric and the magnetic field primarily outside

length of the rutile tube, were equal to 4.5 mm. Under these conditions, the volume of the rutile fills about half of the volume of the resonator. We call this structure a dielectric tube resonator (DTR).

Immediately, it is seen that the total volume of the structure is about 1000 times less than the volume of a TE_{011} cavity with $D/L = 1$. This paper focuses on optimization of EPR performance for sample sizes that can be set anywhere in this $1000\times$ range from exceptionally small to conventional X-band EPR dimensions. It is also apparent that the electric field energy is mostly stored in the dielectric. The rf magnetic field goes to zero and reverses sign near the middle of the tube wall. Thus, one can expect relatively low spurious signal intensity from impurities in the rutile. Remarkably, the useful rf magnetic field in the field plots shown in Fig. 1 is of the order of a millimeter diameter and a millimeter length, and is fairly uniform over this volume.

This paper is primarily concerned with aqueous biological samples that can be classified as saturable and limited in availability. However, the word "limited," although referring to a particular experiment, can vary widely across experiments

from about 20 nL to 20 μL. Presently, the LGR is the preferred sample structure at frequencies below about 35 GHz, and both LGRs and cavity resonators have been used at W-band (94 GHz). The DR offers potential advantages over the LGR, although in our hands, it seems that single-crystal DRs are strongly advantageous over aggregate DRs. The DTR design provides a means of adjusting the sensitivity over a range of sample volumes in a manner that is conceptually similar to adjusting the diameter of the sample loop of an LGR.

The uniform field (UF) DTR is introduced in this paper. It is generally true for the TE_{011} mode that a radius can be found where the mode is cutoff. A mode in a waveguide section, which we call "the central section," can be cutoff if the section is properly terminated at each end. Then, a resonant cavity can be created with the rf fields in the central section exhibiting strict uniformity along the axis of the cavity. UF resonators were introduced in Refs. [34–38]. We can now report that the same approach can be applied to the DTR. It is noted that uniform fields in DRs are not known.

Other potential benefits that have occurred to us include the following:

- The proposed geometry is natural for samples in capillaries or small tubes. The length of the active region of the sample can be preset over a wide range.
- Through choice of the dielectric constant and tube wall thickness, resonators can be fabricated for optimum signal-to-noise ratio for samples across a range of desired size or volume.
- A standard 25 mm diameter cylindrical resonator could be fabricated for insertion in a Dewar. It is noted that this geometry has been found to be convenient for LGRs.
- Extension of the technology to higher frequencies, Q-band (35 GHz), for instance, would lead to increased sensitivity for exceptionally small samples.
- Very high values of the resonator efficiency parameter Λ can lead to new experiments and uniformity of the field along a sample tube can improve the quality of data at all values of H_1.

Analytical equations for calculation of rf magnetic and electric fields in the DTR geometry shown in Fig. 1 have been derived. These equations are cross-checked by finite-element numerical solutions of Maxwell's equations, and consistency is demonstrated. The methodology provides a framework of optimization of resonator design prior to the very costly next stage—actual fabrication.

2 Methods

2.1 Analysis of the DTR

The finite-element simulations were done using ANSYS High-Frequency Structure Simulator (HFSS) (Canonsburg, PA) version 17.1 running on a Dell Precision Tower 7910 with 24 Intel Xeon dual-core processors with hyper-threading and 512 GB of RAM. Insights gained from finite-element simulations can often be used to develop analytic solutions. The two perspectives can be leveraged to provide

further intuition for discovery. Analytic solutions for the electromagnetic fields for the DTR TE$_{011}$ mode in the partially filled cavity shown in Fig. 1 were obtained using the methods outlined in Refs. [39, 40]. It is noted that higher order TE$_{0n1}$ modes can be found from solutions with larger cavity radius. Using the cylindrical coordinates r, θ, z, and the boundaries $-L/2 < z < L/2$ and $r < R$ for the metallic walls and $a < r < b$ for the dielectric, we have, for the z component of magnetic field,

$$H_z = \psi_1 \cos kz, \quad 0 < r < a, \tag{4}$$

$$H_z = \psi_2 \cos kz, \quad a < r < b, \tag{5}$$

$$H_z = \psi_3 \cos kz, \quad b < r < R. \tag{6}$$

In these expressions, the scalar function takes the form

$$\psi_1 = H_0 J_0(\gamma_1 r), \quad 0 < r < a, \tag{7}$$

$$\psi_2 = A J_0(\gamma_2 r) + B N_0(\gamma_2 r), \quad a < r < b, \tag{8}$$

$$\psi_3 = C J_0(\gamma_1 r) + D N_0(\gamma_1 r), \quad b < r < R, \tag{9}$$

where H_0 is the axial magnetic field amplitude in the center of the cavity, J and N are the Bessel functions of the first and second kind, respectively, and the radial wavenumbers are given by

$$\gamma_1 = \sqrt{\frac{\omega^2}{c^2} - k^2}, \tag{10}$$

$$\gamma_2 = \sqrt{\frac{\omega^2}{c^2} \epsilon_r - k^2}. \tag{11}$$

In Eqs. (10) and (11), the radian frequency $\omega = 2\pi f$, c is the speed of light in vacuum, and ϵ_r is the relative dielectric constant of the tube material. For the TE$_{011}$ mode, the axial wavenumber $k = \pi/L$. The radial wavenumber in the dielectric γ_2 is always a positive real number. However, it is interesting to note from Eq. (10) that when the axial length of the cavity L is less than half a free-space wavelength $c/(2f)$, the radial wavenumber γ_1 is imaginary, implying an evanescent radial standing wave in the vacuum regions of the cavity. This effect is seen in the rf magnetic fields shown in Fig. 1b, d. Evanescent standing waves occur outside a DR for the TE$_{01\delta}$ mode [18] but do not occur in a free-space cavity because the minimum L is $c/(2f)$ (obtained as $R \to \infty$). Using this formalism, it is possible to model a UF mode [34–38] in the central section of a UF cavity by setting $k = 0$.

The transverse fields in the DTR cavity are obtained from transverse gradients of the scalar function ψ,

$$H_r = H_0 \frac{k}{\gamma_1} J_1(\gamma_1 r) \sin kz, \quad 0 < r < a, \tag{12}$$

$$H_r = \frac{k}{\gamma_2} [A J_1(\gamma_2 r) + B N_1(\gamma_2 r)] \sin kz, \quad a < r < b, \tag{13}$$

$$H_r = \frac{k}{\gamma_1}[CJ_1(\gamma_1 r) + BN_1(\gamma_1 r)]\sin kz, \quad b < r < R, \tag{14}$$

$$E_\theta = H_0 \frac{i\omega\mu_0}{\gamma_1} J_1(\gamma_1 r)\cos kz, \quad 0 < r < a, \tag{15}$$

$$E_\theta = \frac{i\omega\mu_0}{\gamma_2}[AJ_1(\gamma_2 r) + BN_1(\gamma_2 r)]\cos kz, \quad a < r < b, \tag{16}$$

$$E_\theta = \frac{i\omega\mu_0}{\gamma_1}[CJ_1(\gamma_1 r) + BN_1(\gamma_1 r)]\cos kz, \quad b < r < R, \tag{17}$$

where $i = \sqrt{-1}$ and μ_0 is the magnetic permeability of free space. The constants A, B, C, and D are obtained by matching the components of magnetic field H_z and the electric field E_θ tangent to the dielectric boundaries across $r = a$ and $r = b$.

Closed-form analytic expressions for A, B, C, and D in terms of a, b, γ_1, and γ_2 were obtained using Mathematica (ver. 11.0.1, Wolfram, Somerville, MA). The expressions are lengthy. The eigenmode solution is obtained by setting the electric field component tangential to the cavity wall to zero at $r = R$, Eq. (17). Solutions were obtained for $L = 2R$, for example, by choosing the dielectric material and the dimensions a and b, fixing the frequency to 9.5 GHz, and solving for R. The solutions were checked by inspection of plots of H_z and E_θ over $0 < r < R$ and by comparison with finite-element simulations. The FindRoot program in Mathematica was used to find R. By providing two initial guesses of R (e.g., $0.9R_g$ and $0.95R_g$), the program avoids the use of derivatives in the evaluation and the solutions converge rapidly and consistently. The search was bounded to $b < R < R_0$, where R_0 is the no-dielectric cavity radius. The last solution for R was used to calculate the initial guesses for the next solution as the average tube radius $r_{av} \equiv (a+b)/2$ and tube thickness $t \equiv b - a$ were scanned. Because γ_1 can be imaginary or real, the Bessel functions were of imaginary or real argument. The method produced 3000 eigenmodes in a few seconds.

The power loss in the cavity walls was found by integrating the tangential magnetic fields over the cavity wall surfaces,

$$P_{lw} = \frac{\pi}{2\sigma\delta}\left[4\int_0^R |H_r(z = L/2)|^2 r dr + RL|\psi_3(R)|^2\right], \tag{18}$$

where σ is the conductivity of the cavity walls and the skin depth $\delta = (\pi f \mu_0 \sigma)^{-1/2}$. Note that $\sin kz = 1$ in the expressions for $H_r(z = L/2)$, Eqs. (12–14). The power loss in the dielectric was found by integrating the electric field in the dielectric,

$$P_{ld} = \frac{\pi\omega^3}{2k^2} L\mu_0^2 \epsilon_0 \epsilon_r \tan d \int_a^b |H_r(z = L/2)|^2 r dr, \tag{19}$$

where ϵ_0 is the electric permittivity of free space and $\tan d$ is the dielectric loss tangent. The stored energy in the cavity was found by integrating the electric field over the cavity volume,

$$U = \frac{\pi\omega^2}{2c^2k^2}\mu_0 L\left[\int_0^a |H_r(z = L/2)|^2 r\mathrm{d}r + \epsilon_r \int_a^b |H_r(z = L/2)|^2 r\mathrm{d}r + \int_b^R |H_r(z = L/2)|^2 r\mathrm{d}r\right].$$

(20)

The three unique integrals in Eqs. (18–20) were expressed in closed form and evaluated numerically using Mathematica. From these expressions, the Q value and resonator efficiency (G/W$^{1/2}$) were determined,

$$Q = \frac{\omega U}{P_{lw} + P_{ld}},$$

(21)

$$\Lambda = \frac{\mu_0 10^4}{2\sqrt{P_{lw} + P_{ld}}}.$$

(22)

In Eq. (22), the peak magnetic field in the center of the cavity H_0, Eq. (7), is set to 1 G. For the finite-element simulations, the calculation of Λ was generalized to include sample losses. Using the analytic solutions, contour plots were made of Λ as a function of r_{av} and t for quartz ($\epsilon_r = 3.78, \tan d = 10^{-4}$) [41], sapphire ($\epsilon_r = 8.6, \tan d = 7.5 \times 10^{-5}$) [41], and single-crystal (SC) rutile ($\epsilon_r = 86, \tan d = 8.5 \times 10^{-5}$) [42] using silver cavity walls ($\sigma = 6.17 \times 10^{-7}$S/m). SC rutile can be obtained from MTI Corporation (Materials Tech. Intl., Richmond, CA).

Both sapphire and SC rutile are birefringent, and the value of the dielectric constant perpendicular to the optic axis was used in the r, θ plane. This is the only crystal orientation in the cavity that permits E_θ to be independent of θ. In each case, r_{av} was started at its smallest value, t was scanned from minimum to maximum and then r_{av} was incremented to the next value. Each time r_{av} was started, initial R values close to 20 mm (R_0) were chosen. Each time t increased, the previous solution for R was used for the starting guess. As t increased, R became closer to b, eventually reaching no solution. Outside the colored region of the contour plots, the DTR TE$_{011}$ mode does not exist either because the ID of the tube goes to zero (on the left) or because the cavity OD approaches the dielectric OD. The plots contain 3512, 829, and 3325 data points, respectively. The data for the plots took less than 6 min to calculate. The numerical integrals were the most time-consuming part of the calculation.

2.2 Uniform Field DTR

Determination of a UF DTR structure begins with an HFSS simulation of electromagnetic fields in a DTR, similar to that shown in Fig. 1. The conducting walls are modified using the methods in Refs. [34–38] to produce axially uniform rf fields in the central section of the cavity. First, the radius of the cavity walls in the central section is set to produce cutoff ($k = 0$) for axial circular TE$_{01}$ wave propagation. The radius is then calculated using the analytic methods described above. Next, a central section with this radius is modeled in ANSYS HFSS with perfect magnetic boundaries on each end. The fields should then be axially uniform at 9.5 GHz, which can be confirmed by calculation. Next, a cavity comprising two

end sections butted together but having a metallic septum of the same radius as the central section is created. The axial length of the end section can be set to approximately half the $D/L = 1$ cavity length and the radius increased until the resonance frequency of the structure matches the cut-off frequency, 9.5 GHz. Once this shape is found, the length of the central section is arbitrary. Extending the septum axial length creates the central section.

3 Results

3.1 The Dielectric Tube Resonator

Figure 1 shows HFSS simulations of the rf fields in a $D/L = 1$ DTR cavity partly filled with polycrystalline rutile ($\epsilon_r = 100$ and tan $d = 10^{-3}$) [41]. Polycrystalline rutile can be obtained from TCI Ceramics, Inc. (Bethlehem, PA), an affiliate of National Magnetics Group, Inc. Although the dielectric occupies 49.4% of the volume, the structure is 1/790th in volume (1/9.2 in linear dimension) compared to the TE_{011} cavity with no dielectric. With no sample as shown, $\Lambda = 9.06 \, G/W^{1/2}$, $Q = 826$, and $f = 9.67$ GHz. The dielectric losses are 4.7 times larger than the (silver) wall losses. In comparison, for a TE_{011} cavity with no dielectric at 9.5 GHz, $\Lambda = 2.49 \, G/W^{1/2}$ and $Q = 31, 600$. In Fig. 1b and, especially, d, the evanescent behavior of the magnetic field outside the dielectric, where the field strength increases with radius, is apparent; see Sect. 2.

Figure 2 shows the DTR Λ value as a function of r_{av} and t for quartz, sapphire, and SC rutile tubes as predicted by the analytic methods. The values for the dielectric constants and loss tangents are given in Sect. 2. The minimum r_{av} values for the plots are (0.375, 0.25, and 0.1) mm for quartz, sapphire, and SC rutile, respectively, while corresponding minimum t values are (0.05, 0.1, and 0.1) mm. In each of the plots, t was increased at fixed r_{av} until either the ID of the tube went to zero, or R became equal to the outer radius of the tube b. Consequently, the contours cover the full parameter space (for $D/L = 1$) of the DTR TE_{011} mode. For each plot, it is apparent that the maximum Λ tends to occur for the smallest tube ID and the largest wall thickness. As t approaches zero, Λ approaches that of the TE_{011} cavity with no dielectric, $2.49 \, G/W^{1/2}$. Λ values smaller than this occur for large tube IDs and a relatively large t.

The contour plots shown in Fig. 2 permit determination of the dimensions of the dielectric in an initial estimate. Figure 3 can then be used to determine the inner dimension of the metallic cylinder that is required to achieve microwave resonance at 9.5 GHz. The process can be repeated until an acceptable trade-off has been found. Design and construction of a practical resonator can then proceed. Together, Figs. 2 and 3 provide design information for a DTR. In addition, if a dielectric tube is readily available, these contour plots permit development of a DTR with a predictable Λ value.

A high Λ value usually is accompanied by the constraint of small sample volume. If a larger sample is required to be examined, the contour plots provide guidance for development of a dedicated DTR for an optimum signal-to-noise ratio for that class

Fig. 2 Contour plots of the resonator efficiency as a function of the average tube radius r_{av} and thickness t (see Sect. 2) for **a** quartz, **b** sapphire, and **c** SC rutile tubes in a $D/L = 1$ cavity. The cavity radius was calculated for the fixed frequency of 9.5 GHz
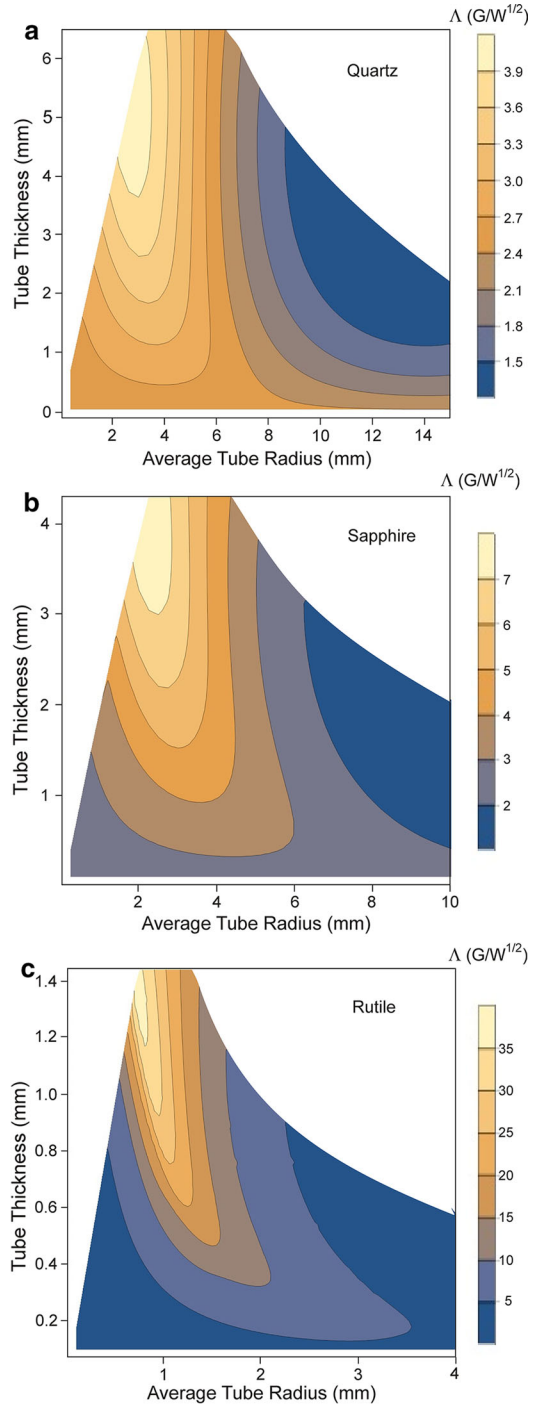
Fig. 3 Contour plots of the
cavity radius as a function of
the average tube radius r_{av} and
thickness t (see Sect. 2),
corresponding to the resonator
efficiencies shown in Fig. 2 for
**a** quartz, **b** sapphire, and **c** SC
rutile
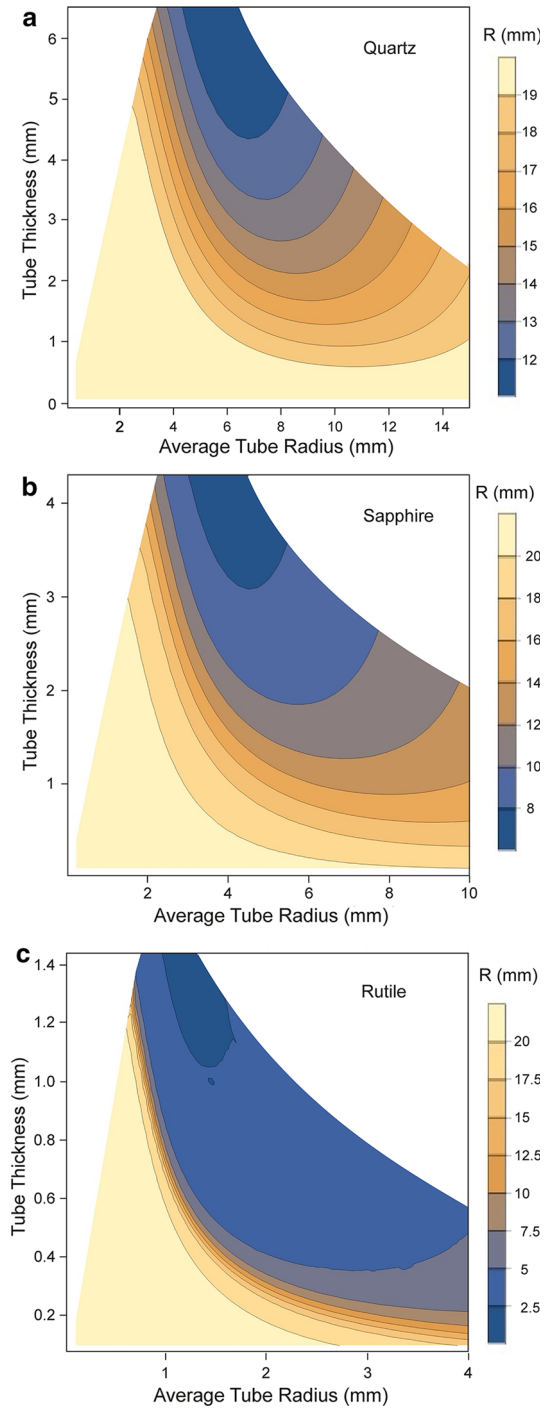
of samples. A resonator with somewhat higher Λ value and with reasonable sample size may be suitable for general purpose usage, noting that the signal-to-noise ratio depends both on Λ and sample volume.

In Fig. 4, the D/L of the DTR cavity was varied for fixed tube dimensions that correspond to the maximum Λ obtained for sapphire $D/L = 1$, as shown in Fig. 5 (7.74 G/W$^{1/2}$). The maximum Λ is about 8% larger (8.35 G/W$^{1/2}$) for the same tube with the cavity D/L of approximately 1.9.

The DTR geometry of a tube with a constant radial cross section extending axially from wall to wall of the cavity does not produce as large Λ as the geometry of a solid dielectric cylinder with $D/L = 1$ placed in a cavity. Using the methods in Ref. [18], the electromagnetic fields of the TE$_{01\delta}$ mode in a dielectric cylinder can be calculated analytically and used to determine Λ. Since the fields are evanescent outside the dielectric, a natural analytic limit is to neglect the power losses in the cavity walls. Values of Λ for a DR for SC rutile, sapphire, and quartz are shown in Table 1 along with the Q value and OD of the dielectric. These represent benchmark Λ (and Q) values that can be compared to the DTR analytic results, as shown in Table 1. For $D/L = 1$, the DTR has a lower Λ value than the DR by about 27% for sapphire but about 42% for SC rutile.

Because of the high loss tangent of water, the presence of aqueous sample causes Λ to decrease. The effect of aqueous sample and a sample tube was quantified in the DTR using ANSYS HFSS. For water at 9.5 GHz, $\epsilon_r = 63, \tan d = 0.42$ was used [43]. Two different extruded polytetrafluoroethylene (PTFE) sample tubes available from Zeus Industrial Products, Inc. (Orangeburg, SC) were used. The ID of the American Wire Gauge (AWG) 30 standard wall (sw) sample tube is 0.305 mm and the ID of the AWG 26 light wall (lw) sample tube is 0.457 mm. The OD of both the AWG26lw and AWG30sw tubes is 0.762 mm. The ID of the SC rutile tube is 0.8 mm, and the ID of the sapphire tube is 1 mm. It is seen that the aqueous sample decreases the Λ values by 30–60% for the SC rutile tube, but only by about 17% for the sapphire tube for the larger sample. The corresponding Q values are also shown. For the HFSS simulations, we also report the sample volumes and saturable EPR signals integrated over the sample volume [44, 45]. As described in Ref. [45], the formula for calculating the saturable signal is given by

Fig. 4 Resonator efficiency as a function of D/L for sapphire with $r_{av} = 2.25$ mm and $t = 4.3$ mm. This corresponds to $\Lambda = 7.74$ G/W$^{1/2}$ for $D/L = 1$ and $R = 10.91$ mm. R increases very rapidly as D/L increases beyond the values shown
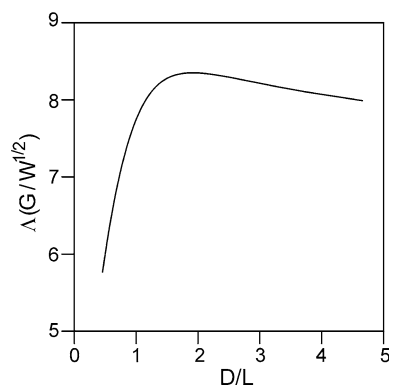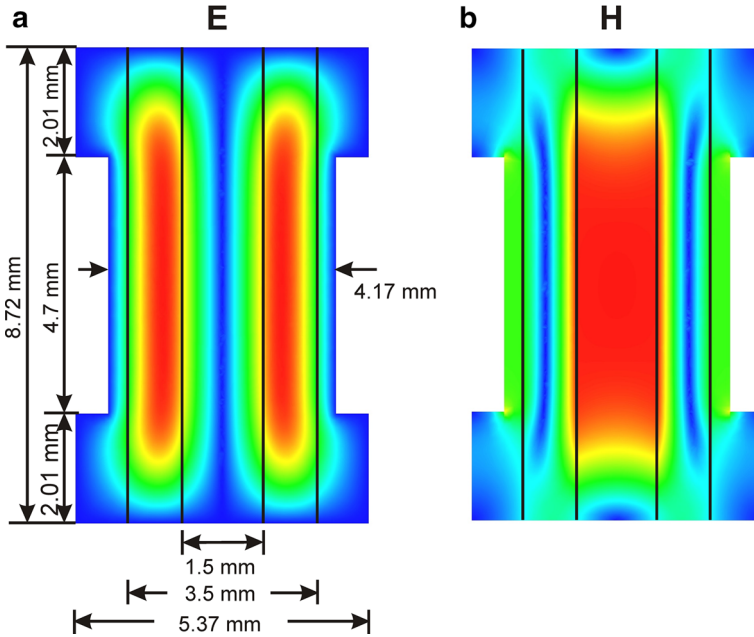
Fig. 5 Cross-sectional views of the magnitude of **a** electric field and **b** magnetic field inside a metallic cavity designed with two end sections that support an axially uniform rf field in the central section. The polycrystalline dielectric tube extends uniformly along the axial extent of the structure

Table 1 Dielectric resonator properties with $D/L = 1$

Description	Material	Λ (G/W$^{1/2}$)	V_s (μL)	S_s (V)	Q	dOD (mm)
DR	SC rutile	54.8	–	–	11,800	2.88
DTR	SC rutile	31.9	–	–	9900	2.80
DTR w/AWG30sw	SC rutile	23.0	0.67	3.58	4920	2.80
DTR w/AWG26lw	SC rutile	13.3	1.51	4.57	1590	2.80
DR	Sapphire	10.4	–	–	13,300	9.07
DTR	Sapphire	7.56	–	–	11,600	9.00
DTR w/AWG26lw	Sapphire	6.31	3.36	4.53	6960	9.00
DR	Quartz	4.87	–	–	10,000	13.61

$$S_s = \frac{\omega \int H_{1r}^2 dV_s}{10^4 H_{1r\max} \sqrt{P_l}}, \tag{23}$$

where r stands for the rotating component, the power losses include cavity walls, dielectric, sample, and sample holder, and the integral is over the sample volume. Compare to Eq. (22). Note that the integrated signal can be larger due to a larger sample volume even with a lower resonator Λ value.

### 3.2 The Uniform Field Dielectric Tube Resonator

Figure 5 shows a UF structure that was developed from the DTR structure of Fig. 1. It contains a polycrystalline rutile tube of the same radial cross section as shown in Fig. 1, but the conducting walls were modified as described in Sect. 2.2. until the resonance frequency of the structure matched 9.5 GHz. In Fig. 5b, evanescent magnetic fields are seen in the end sections. For this structure, $\Lambda = 5.21\,\text{G}/\text{W}^{1/2}$, $Q = 782$, and $f = 9.52$ GHz.

Figure 6 compares analytic solutions of the rf fields in the axial center of the DTR cavities of Figs. 1 and 5 as a function of radius. The rf magnetic fields of the $D/L = 1$ cavity are evanescent, whereas the fields in the central section of the UF cavity are not, which is consistent with Eqs. (10) and (11) and $k = 0$ for the central section UF; see Sect. 2.

Synthetic sapphire tubes are available from Saint-Gobain Crystals [46]. A tube suitable for EPR use has an ID of 2 mm and an OD of 7 mm. When a DTR is made from this, $\Lambda = 6.4\,\text{G}/\text{W}^{1/2}$ with a cavity radius 18.6 mm with no sample. If another tube of ID 8 mm and OD 9 mm is placed around the smaller tube, $\Lambda = 6.9\,\text{G}/\text{W}^{1/2}$ with a cavity radius 10.7 mm with no sample. This is a double DTR. The Λ value of the dual DTR is somewhat smaller than a solid DTR of the same ID and OD, 7.5 $\text{G}/\text{W}^{1/2}$, which is expected due to the air gap between tubes. Simulations of electromagnetic fields in a UF version of the double DTR are shown in Fig. 7. Table 2 shows results from ANSYS HFSS simulations of a UF double DTR central section only (perfect magnetic boundaries were used on each end) as sample size is varied. The central cavity section has an OD of 17.4 mm and $D/L = 1$. PTFE extruded tubes available from Zeus were used. One can see the integrated sample signal peaks for the AWG20sw tube for a sample size of about 10 μL. When end sections are added, the results do not change much, $\Lambda = 2.1\,\text{G}/\text{W}^{1/2}$, $S_s = 7.89$ V with $Q = 1730$. The electric and magnetic fields are similar to those shown in Fig. 1, although both fields are more confined in the tubes than those shown in Fig. 1. It is concluded that UF versions of all DTRs can be found.
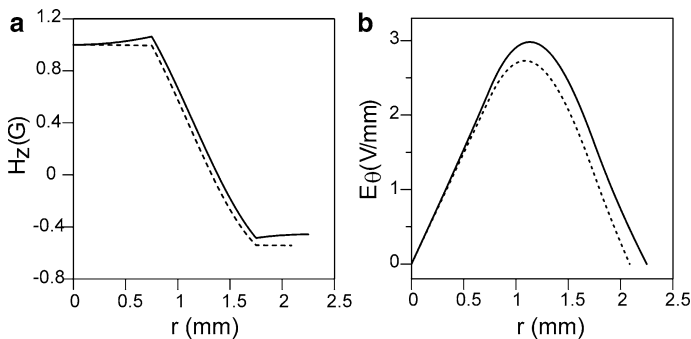
Fig. 6 Comparison of the peak **a** axial magnetic field and **b** azimuthal electric field in the cavity center as a function of radial position in the cavity of Fig. 1 (*solid*) and the central section of Fig. 5 (*dashed*)
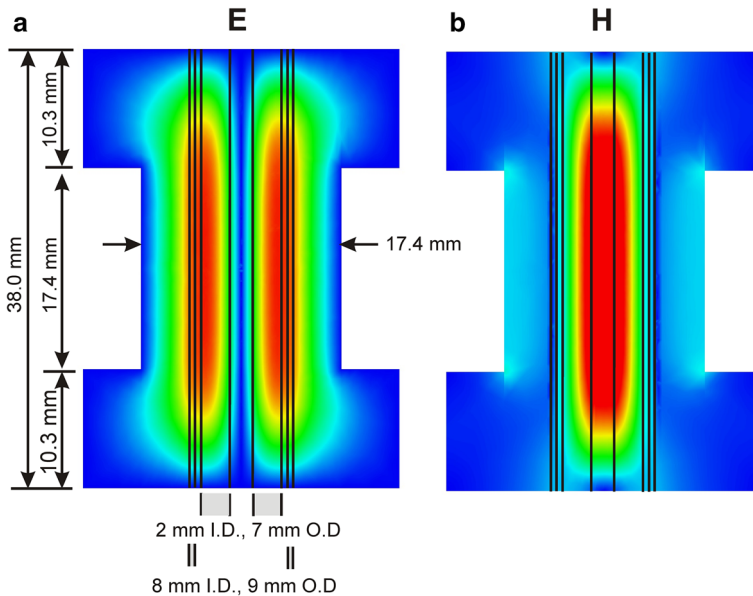
Fig. 7 Cross-sectional views of the magnitude of **a** electric field and **b** magnetic field inside a metallic cavity designed with two end sections that cause an axially uniform rf field in the central section. The nested sapphire dielectric tubes extend uniformly along the axial extent of the structure, which is a UF double DTR

Table 2 UF double DTR central section properties with $D/L = 1$

Sample tube	ID (mm)	OD (mm)	f (GHz)	Q	Λ (G/W$^{1/2}$)	V_s (μL)	S_s (V)
None	–	–	9.506	10,300	5.35	–	–
AWG26sw	0.46	0.91	9.505	6620	4.53	2.85	5.70
AWG24sw	0.56	1.17	9.504	4530	3.86	4.26	6.99
AWG22sw	0.71	1.32	9.502	2300	2.85	6.89	8.01
AWG20sw	0.86	1.68	9.496	1150	2.16	10.2	8.12
AWG18sw	1.07	1.88	9.484	486	1.54	15.5	7.88
AWG16lw	1.35	1.65	9.455	173	1.02	24.7	7.51

4 Discussion

Three materials with low microwave dielectric loss, quartz, polystyrene (and the cross-linked variant, Rexolite), and Teflon, have been inserted into microwave cavities for many years for use as sample tubes, Dewars, and various technical devices. They were generally considered as perturbing elements that slightly shifted the resonant frequency to lower values but did not otherwise alter the microwave fields in the cavity. However, we are aware of two papers describing the

introduction of dielectrics in microwave cavities that changed the microwave fields very substantially. Mett et al. [18] analyzed the introduction of a small crystal of $KTaO_3$, which has a high dielectric constant and was, in fact, a DR, into a resonant TE_{011} cavity. Strong coupling between the two resonant circuits gave rise to two modes, with RF magnetic fields parallel and antiparallel. In a second paper, Mett, Froncisz, and Hyde [34] introduced the concept of the axial UF TE cavity, which consists of three sections: a central section at cutoff and two end sections containing dielectric material as required to set up the cut-off standing wave. The DTR and UF DTR cavities can be considered as a third paper in this series on the introduction of dielectric structures into cavities. It considers the effect of a dielectric tube, which may have a significant wall thickness, on the TE_{011} cavity mode.

The DTR is a hybrid structure that lies between the extremes of a pure DR and a pure cylindrical TE_{011} cavity resonator. A pure-mode cavity is often appropriate at X-band when relatively large volumes of sample are available. The techniques of this paper are appropriate when smaller volumes of sample are available. In this perspective, the ΛV product, where V is the sample volume, can be optimized for specific sample classes. It also offers several technical advantages over the pure-mode geometry. Perhaps foremost is the convenience of coupling and matching of a TE_{011} cavity in combination with the high Λ values that are provided by the pure DR. In addition, the cylindrical metallic walls of the DTR provide a shield that eliminates microwave radiation.

A substantial toolbox has been developed for use with pure cylindrical resonators that includes managing eddy currents induced by incident field modulation by forming the walls by the wire-wound technique [30, 47] or by use of modulation slots [48, 49]. Capacitive coupling to a waveguide offers advantages over inductive coupling [50]. An alternative coupling strategy has been introduced that uses semirigid coaxial cables [33]. Several types of automatic frequency control have been published [51], and designs for handling small sample tubes have been described [52]. Having completed the initial analysis in the present paper, we expect to deploy this toolbox to arrive at a practical resonator.

The contour plots, Figs. 2 and 3, are intended to aid the reader in the design of a DTR resonator that is configured to satisfy specific constraints. The variables are the dielectric constant, which must be that of quartz, sapphire, or rutile; the inner and outer diameters of the dielectric, which allow calculation of the wall thickness and the average diameter; and the inner diameter of the surrounding metallic enclosure. The plots can be used in several ways. If highest possible Λ value is desired, it is apparent that rutile should be used, the inner diameter should be as small as possible, and the outer diameter of the dielectric should coincide with the inner diameter of the metal cylinder. If one starts with an available dielectric tube with inner and outer radii known, the plots immediately yield the outer metallic diameter and the Λ value. The contour plots can also be used to design a resonator that will fit an available immersion Dewar. Development of a general purpose DTR would start with assumptions about the size or volume of the sample and a decision about which of the three dielectrics to use. The outer diameter of the dielectric and the inner diameter of the metal cylinder could then be determined.

Design of a UF DTR begins using the contour plots to arrive at the DTR, followed by HFSS adjustment of the diameter of the metal enclosure to achieve the cut-off frequency. Finite-element modeling is needed for precise design of the end sections because of the perturbation of fields by the septa.

An incidental benefit of the sapphire DTR and UF DTR resonators is that they can be sufficiently small that they can be conveniently immersed into a temperature-controlled gas environment—noting that the counterpart free-space resonators are large relative to the available space in most EPR magnets. The good thermal conductivity of sapphire makes it a favorable dielectric for use in an immersion temperature control system. It is, however, noted that to achieve good quantitative accuracy with a UF DTR, a metallic shield over the sample as it passes through the end regions of the UF coil should be employed [52]. It is concluded that sapphire is a good candidate for development of a general purpose UF DTR. In addition, it seems likely that PTFE extrusions can be developed for the DTR that enhance sensitivity for aqueous samples. Such extrusions can be expected to alter the performance of the UF DTR, but probably by an acceptable amount.

The UF DTR seems likely to contribute to the technology of quantitative EPR because of the good uniformity of the RF magnetic field over the sample. Among the experiments where nonlinear EPR experiments are adversely affected by the nonuniformity of the microwave field across the sample are the following: (1) tip angle variation across the sample in pulse EPR; (2) variation of the sample response in long-pulse vs short-pulse saturation recovery EPR; (3) free induction decay; (4) continuous wave saturation; (5) smearing out of the saturation transfer "passage" response because of variation of saturation across the sample, and (6) ELDOR (electron–electron double resonance).

The rutile DTR should be thought of as a miniature TE_{011} resonator that yields X-band sensitivity for small samples that may approach that of high-frequency EPR spectrometers. Although high field has the advantage of increased Zeeman interaction, linewidths also tend to increase with field strength. The capability of being able to examine small samples at two or more frequencies—say X- and W-band—may, it is conjectured, enable the separation of Zeeman and hyperfine interactions. A specific example in this category that is of considerable interest in this laboratory is provided in Ref. [53], "Spin-label W-band EPR with seven-loop-six-gap resonator, application to lens membranes derived from eyes of a single donor."

References

1. R.C. Rempel, C.E. Ward, R.T. Sullivan, M.W. St. Clair, H.E. Weaver, "Gyromagnetic resonance method and apparatus," U.S. Pat. 3,122,703 (1964)

2. J.S. Hyde, G.R. Eaton, S.S. Eaton, Concepts Magn Reson. Part A Bridg. Educ. Res. **28A**, 85–86 (2006)
3. L.G. Stoodley, J. Electron Control. **14**, 531–546 (1963)
4. J.S. Hyde, J. Chem. Phys. **43**, 806–1818 (1965)
5. J.S. Hyde, "Microwave cavity resonator", U.S. Pat. 3,250,985 (1966)
6. W.M. Walsh Jr., L.W. Rupp Jr., Rev. Sci. Insrum. **57**, 2078–2279 (1986)
7. R.W. Dykstra, G.W. Markham, J. Magn. Reson. **69**, 350–355 (1986)
8. A. Sienkiewicz, K. Qu, Rev. Sci. Instrum. **65**, 68–74 (1994)
9. M. Jaworski, A. Sienkiewicz, C.P. Scholes, J. Magn. Reson. **1969–1992**(124), 87–96 (1997)
10. I.N. Geifman, I.S. Golovina, V.I. Kofman, R.E. Zusmanov, Ferroelectrics **234**, 81 (1999)
11. A. Sienkiewicz, M. Jaworski, B.G. Smith, P.G. Fajer, C.P. Scholes, J. Magn. Reson. **143**, 144–152 (2000)
12. Y.E. Nesmelov, J.T. Surek, D.D. Thomas, J. Magn. Reson. **153**, 7–14 (2001)
13. A. Blank, E. Stavitski, H. Levanon, F. Gubaydullin, Rev. Sci. Instrum. **74**, 2853–2859 (2003)
14. S.M. Mattar, A.H. Emwas, Chem. Phys. Lett. **368**, 724–731 (2003)
15. I.N. Geifman, I.S. Golovina, Concepts Magn. Reson. **26B**, 46 (2005)
16. A. Sienkiewicz, B. Vileno, S. Garaj, M. Jaworski, L. Forró, J. Magn. Reson. **177**, 261–273 (2005)
17. I.S. Golovina, I.N. Geifman, A. Belous, J. Magn. Reson. **195**, 52–59 (2008)
18. R.R. Mett, J.W. Sidabras, I.S. Golovina, J.S. Hyde, Rev. Sci. Instrum. **79**, 094702 (2008)
19. S.M. Mattar, S.Y. Elnaggar, J. Magn. Reson. **209**, 174–182 (2011)
20. A. Raitsimring, A. Astashkin, J.H. Enemark, A. Blank, Y. Twig, Y. Song, T.J. Meade, Appl. Magn. Reson. **42**, 441–452 (2012)
21. S.Y. Elnaggar, R. Tervo, S.M. Mattar, J. Magn. Reson. **238**, 1–7 (2014)
22. S.Y. Elnaggar, R. Tervo, S.M. Mattar, J. Magn. Reson. **242**, 57–66 (2014)
23. S.Y. Elnaggar, R. Tervo, S.M. Mattar, J. Magn. Reson. **245**, 50–57 (2014)
24. S.Y. Elnaggar, R.J. Tervo, S.M. Mattar, J. Appl. Phys. **118**, 194901 (2015)
25. H.Y. Yee, I.E.E.E. Trans, Microwave Theory Tech. **13**, 256 (1965)
26. D.M. Pozar, *Microwave Engineering*, 4th edn. (Addison-Wesley, New York, 1990), secs. 7.5, 7.8
27. M.W. Pospieszalski, I.E.E.E. Trans, Microwave Theory Tech. **27**, 233 (1979)
28. F.J. Rosenbaum, Rev. Sci. Instrum. **35**, 1550–1554 (1964)
29. J.S. Hyde, "EPR spectrometer resonant cavity", U.S. Pat. 3,878,454 (1975)
30. J.S. Hyde, in *Handbook of Microwave Technology*, vol. 2, ed. by T.K. Ishii (Academic Press, New York, 1995), pp. 365–402
31. J.S. Hyde, W. Froncisz, in *Advanced EPR: Applications in Biology and Biochemistry*, ed. by A.J. Hoff (Elsevier, Amsterdam, 1989), pp. 277–306
32. G. Feher, Bell Syst. Tech. J. **36**, 450–483 (1956)
33. W. Froncisz, J.S. Hyde, J. Magn. Reson. **47**, 515–521 (1982)
34. R.R. Mett, W. Froncisz, J.S. Hyde, Rev. Sci. Instrum. **72**, 4188–4200 (2001)
35. J.R. Anderson, R.R. Mett, J.S. Hyde, Rev. Sci. Instrum. **73**, 3027–3037 (2002)
36. J.S. Hyde, R.R. Mett, J.R. Anderson, Rev. Sci. Instrum. **73**, 4003–4009 (2002)
37. J.S. Hyde, R.R. Mett, W. Froncisz, J.R. Anderson, "Cavity resonator for electron paramagnetic resonance spectroscopy having axially uniform field", U.S. Patent 6,828,789 (2004)
38. R.R. Mett, J.W. Sidabras, J.S. Hyde, Appl. Magn. Reson. **31**, 571–587 (2007)
39. S. Ramo, J.R. Whinnery, T. Van Duzer, *Fields and Waves in Communication Electronics* (Wiley, New York, 1965), sec. 8.04
40. J.D. Jackson, *Classical Electrodynamics*, 2nd edn. (Wiley, New York, 1975), sec. 8.3
41. A.R. Von Hippel, *Dielectric Materials and Applications* (Artech House, Boston, 1954)
42. M.E. Tobar, J. Krupka, E.N. Ivanov, R.A. Woode, J. Appl. Phys. **83**, 1604–1609 (1998)
43. W.J. Ellison, J. Phys. Chem. Ref. Data **36**(1), 1–18 (2007)
44. J.W. Sidabras, R.R. Mett, J.S. Hyde, J. Magn. Reson. **172**, 333–341 (2005)
45. J.S. Hyde, J.W. Sidabras, R.R. Mett, Resonators for multifrequency EPR of spin labels [chapter 5.2], in *Multifrequency Electron Paramagnetic Resonance, Theory and Applications*, ed. by S. Misra (Wiley, Berlin, 2011), pp. 244–270
46. Saint-Gobain Crystals. EFG Sapphire Tubes. Milford, NH: n.p. (2006)
47. J.S. Hyde, J. Chem. Phys. **43**, 1806 (1965)
48. R.R. Mett, J.S. Hyde, Rev. Sci. Instrum. **76**, 014702 (2005)
49. R.R. Mett, J.R. Anderson, J.W. Sidabras, J.S. Hyde, Rev. Sci. Instrum. **76**, 094702 (2005)
50. R.R. Mett, J.W. Sidabras, J.S. Hyde, Appl. Magn. Reson. **35**, 285–318 (2008)

51. J.S. Hyde, J. Gajdzinski, Rev. Sci. Instrum. **59**, 1352 (1988)
52. J.W. Sidabras, T. Sarna, R.R. Mett, J.S. Hyde, J. Magn. Reson. **282**, 129–135 (2017)
53. L. Mainali, J.W. Sidabras, T.G. Camenisch, J.J. Ratke, M. Raguz, J.S. Hyde, W.K. Subczynski, App. Magn. Reson. **45**, 1343–1358 (2014)